Petroleum and Coal

Article **Open Access**

Reservoir Characteristics and 3D Static Modelling of the Fana Field, Termit Basin, Niger Republic

Abass Yacoubou Issaka[1], Olugbenga A. Ehinola[2], Oladotun Oluwajana[3], Jerome Asedegbega[4], Alexander Nwakanma[4]*

[1] *Petroleum Geoscience Program, Pan African University Life and Earth Sciences Institute (including Health and Agriculture), University of Ibadan, Ibadan, Nigeria*
[2] *Energy and Environmental Research Group, Department of Geology, University of Ibadan, Nigeria*
[3] *Department of Earth Sciences, Adekunle Ajasin University, Akungba-Akoko, Nigeria*
[4] *GCube Integrated Services Ltd, Lagos, Nigeria*

Received April 4, 2024; Accepted July 19, 2024

Abstract

This study aims to assess the petrophysical characteristics of the reservoirs in the Fana Field of the Paleogene Sokor_1 system of the Termit Basin and generate a 3D static model of the field. This study integrated all the available data, well logs from four exploratory wells, and a 3D seismic section. The five hydrocarbon-bearing units (E_1, E_2, E_3, E_4, and E_5) have been identified. The average petrophysical values of the reservoir in the Paleogene Sokor-1 revealed that E_1 is the best reservoir with low water saturation, good porosity, and excellent permeability. The delineated net-pay thickness of the reservoirs (19.82m, 37.88 m, 55.27 m, 15.26 m, and 23.78 m) was respectively estimated. The effective porosity of the reservoirs was identified to be 20.66 %, 18.79 %, 18.33 %, and 13.15 %. The permeability of the reservoirs (1774.86 mD, 1535.82 mD, 1300.09 mD, 1325.42 mD, and 1339.66 mD respectively) was identified. The water saturation is 28.63 %, 43.70 %, 50.34 %, 61.34 %, and 69.48 % respectively. Stratigraphically, the shale thickness below and above each reservoir can also act as seals for trapping the hydrocarbon accumulation. The seismic interpreted faults trend NW-SW and NNW-SSE. This study showed that the Paleogene Sokor_1 Formation in Termit Basin is an exceptionally promising reservoir with strong indications of significant hydrocarbon-bearing zones..

Keywords: *Petrophysical properties; Atatic model; Hydrocarbon potential; Fana Field; Termit Basin.*

1. Introduction

The NW-SE trending Termit Basin covers an area of 27,000 km^2, located between the Bornu Basin in northeastern Nigeria and the Tefidet, Tenere, Grein, and Kafra grabens (northern Niger Republic). Termit Basin is considered the second largest oil-bearing basin, after the Muglad Basin, in the Central and Western African Rift System (WCARS) [1-5]. The production capacity of the Termit Basin has reached nearly 12 × 10^4 barrels of crude oil per day, while one of the main high-yield oil field discoveries of the Termit Basin is found in the Eocene Sokor-1 Member.

The Fana Field is located in the central part of the Termit Basin, (Figure 1). Hydrocarbons have been discovered in the surrounding fields of the Fana Field namely Goumeri, Jaouro, Abolo, Hadara, Dibeilla, and Kaido Fields. Hydrocarbon production has not started yet in the Fana Field, only exploration activities are ongoing with few exploratory wells.

Several authors have identified the Paleogene Sokor Formation and the Cretaceous Yogou Formation as the two sets of reservoirs, in the Termit Basin, including [2-3, 6-12] considered the Fana low uplift as the most favourable exploration zone in the Termit Basin based on its relatively well-developed fractures for hydrocarbon migration and accumulation.

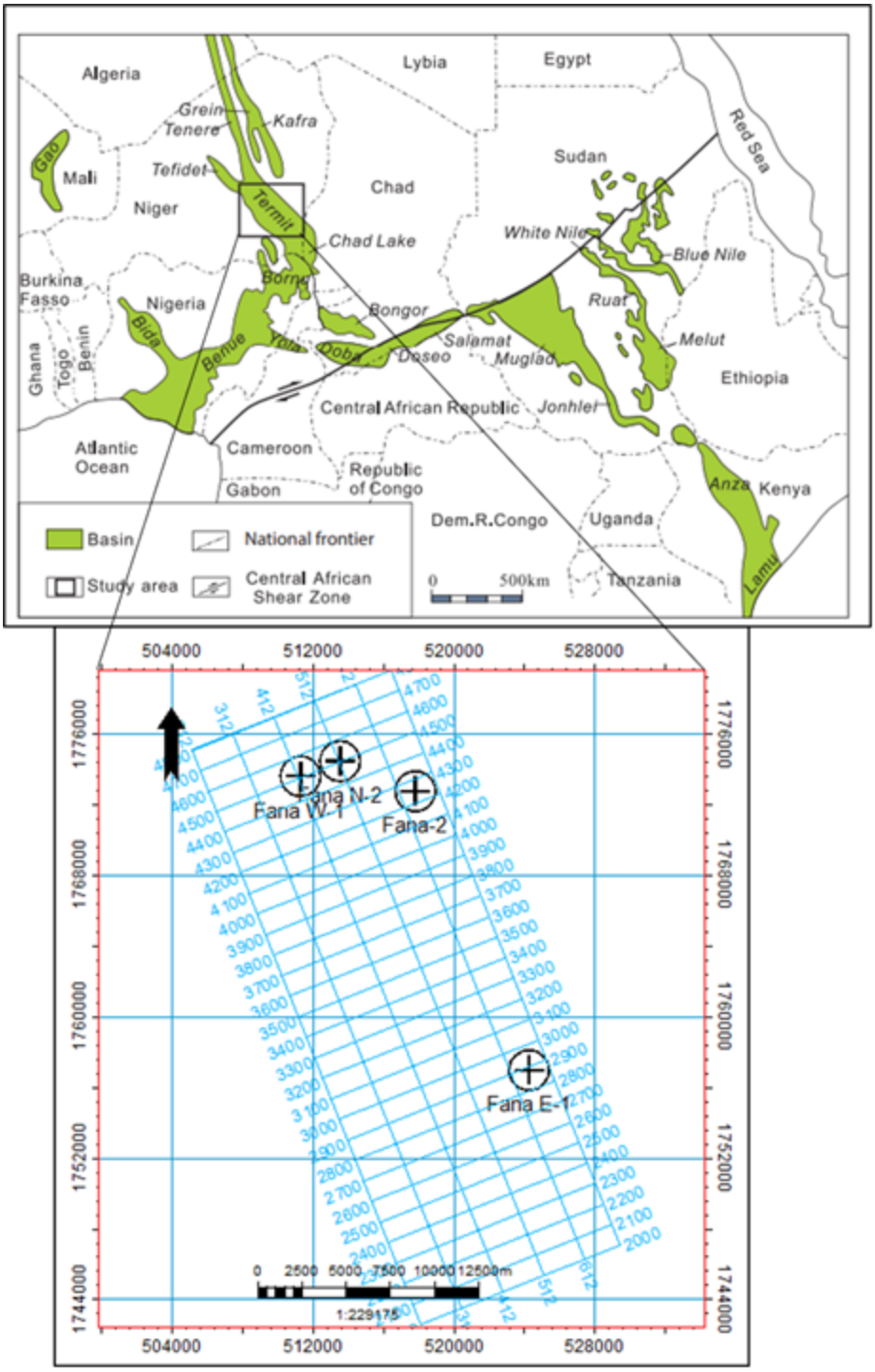

Figure 1. Regional geological map showing (a) indicating the Termit Basin [2], (b) base map showing Fana Field with four wells and the seismic lines.

Therefore, information on the petrophysical properties of the Paleogene Sokor_1 sand-bodies in the Fana Field is rarely discussed in published reports. This study aims to utilize well logs and 3D seismic data to generate robust 3-D reservoir models for the Fana Field of the Termit Basin (Niger Republic), which allows for proper visualization of the heterogeneous nature of the reservoir properties (porosity, permeability, water saturation, and hydrocarbon

saturation) and to improve the understanding of the lateral distribution of the reservoirs and hydrocarbon potential.

Volumetric calculations, well location, production optimization, and reservoir simulation are the core of reservoir modelling [13]. The reservoir model typically comprises dynamic (such as fluid flow) and static (such as lithology and porosity) geological information [13]. The geometry and architecture (property) of hydrocarbon reservoirs adequately define the three-dimensional (3D) modelling [14]. Since the Fana Field is highly attractive for new oil and gas explorations, there is a need in this study for the integration of geological and geophysical data (well logs, seismic data, formation evaluation, and 3D modelling), for the delineation of reservoir geometry and identification of new opportunities in the field.

1.1. Geologic setting of the study area

The Termit Basin is a Mesozoic-Cenozoic superimposed rift basin seated on the Precambrian-Jurassic basement [15]. The Termit Basin, in the southeast of Niger, lies to the north of the Central African shear belt, and geotectonically belongs to the northern branch of the West African rift system [15]. It covers an area of 27,000 km^2 and it contains over 12,000 m thick, which is a large structural depression in the Niger Republic [1].

The eastern part of the Basin, where Fana Field is located, is made up of two distinct tectonostratigraphic areas: an asymmetric rift extensional system with Mesozoic-Cenozoic sedimentary successions on top of a Precambrian Crystalline Basement and a Cambrian-Jurassic epimetamorphic basement [11]. The sedimentary covers in the Termit Basin are composed of the Cretaceous, Paleogene, Neogene, and Quaternary (Figure 2).

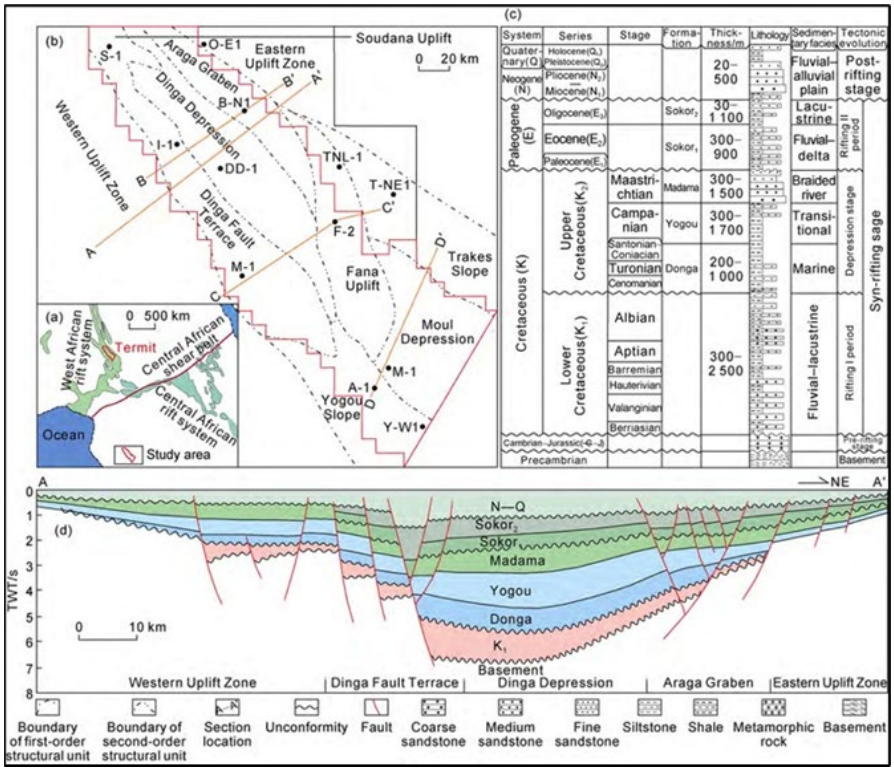

Figure 2. (a) Termit Basin location [2]; (b) Units division of the structural composition of the Termit Basin [20]; (c) Termit Basin's stratigraphic column [21-23]; (d) Formations and seismic section in the Termit Basin [24].

The tectonostratigraphic units of the Termit Basin include five main Formations namely Donga, Madama, Yogou, Sokor-1, and Sokor-2 [1]. The Cenomanian-Coniacian Donga Formation is comprised of marine clastic shale interbedded with thin and fine sand deposits [2].

Comprising broad strata of mudstone and shale, the Campanian-Santonian Yogou Formation is approximated to have a thickness spanning 300 to 1000 m, and is considered a

highly productive source rock in the Niger Rift Basin. The Madama Formation consists of fluvial sandstone, deposited during the Maastrichtian due to regression accompanied by epeirogenic deformation [17]. A 100-200 m thick Madama Formation serves as the top reservoir [17].

The Alternances de Sokor, also known as the Sokor-1 Formation comprised of fluvial deltaic sandstone interbedded with mudstone and shale [18]. The Paleogene-Eocene Sokor-1 Formation sandstones are deposited during the second phase rifting phase. The predominant composition of reservoir rocks in the basin consists mainly of sandstones of the Sokor-2 Formation. Meanwhile, lacustrine mudstones within the same Formation serve as seals [2,19]. The Sokor-2 Formation, with a thickness of 30-1100 m, represents early Oligocene syn-rift lacustrine mudstones discovered in the Termit Basin [2].

2. Materials and methods

3D PSTM seismic data (SEG-Y Format) and a suite of well log data (LAS Format) from four exploratory wells drilled in the Fana Field, Termit Basin were provided by the Centre of Petroleum Documentation (CPD) of the Ministry of Petroleum, Niger Republic.

The details of available log information of each well including check shot data, headers, and well deviation are shown in (Table 1). The 3D PSTM seismic data (SEG-Y Format), recorded in the Koulélé bloc, covers the area of Fana Field in the Termit Basin and was utilized in this study. The 3D seismic data covers an area of about 1500 km^2. The seismic data was acquired with a grid consisting of 5100 inline spaced 12.50 m apart, starting from inline 418 and ending at inline 5518. The crosslines were recorded at intervals of 25 meters, with 800 crosslines ranging from crossline 82 to crossline 88.

Schlumberger (Petrel^{TM}) software was used for the well correlation, seismic interpretation, and 3D modelling of the field. The adopted workflow of the study is shown in (Figure 3). The calculated petrophysical parameters namely net-to-gross (NTG), shale volume (V_{sh}), porosity (Ø), permeability (K), water saturation (S_w), and hydrocarbon saturation (S_h) of the identified reservoirs in four wells were estimated.

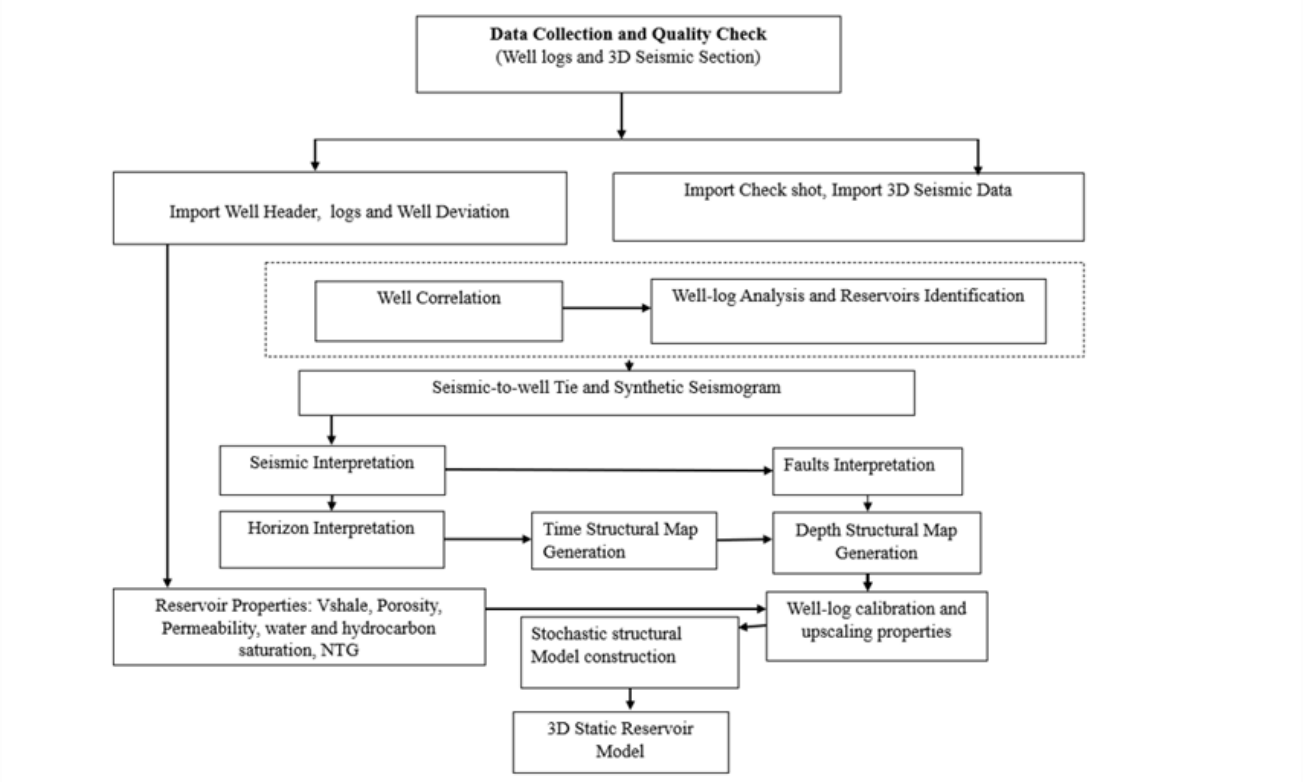

Figure 3. Workflow of the study.

Table 1. Well Logs List of available wells in the Fana field.

Well names		Fana W_1	Fana E_1	Fana N_2	Fana 2
Well headers		✓	✓	✓	✓
Well tops		✓	✓	✓	✓
Deviation		☒	☒	✓	☒
Check shot		☒	☒	✓	☒
Well Logs	Gamma-Ray	✓	✓	✓	✓
	Resistivity	✓	✓	✓	✓
	RHOB	✓	✓	✓	✓
	DT	✓	✓	✓	✓
	Calip	✓	✓	✓	✓
	NPHI	✓	✓	✓	✓

NOTE: Available and unavailable data connotes (x) and (ü) respectively.

2.1. Structural interpretation and 3D modelling

2.1.1. Seismic-to-well tie and seismic interpretation

After the petrophysical evaluation of the reservoir, the sonic log was calibrated using the check shot data of well Fana N_2 and the Riker wavelet method. A wavelet extraction window is used to obtain the extracted wavelet and perform bulk shifting for a precise tie. Bulk shifting was applied during the synthetic seismogram generation at a rate of 10 milliseconds to better match the process seismic with well-log across the five reservoirs (E_1, E_2, E_3, E_4, and E_5) of the wells in the Fana Field. The variance volume attribute has been applied to the seismic section to improve fault trace along the time slice (Z= -5998.00 m), which also assisted to improve the quality of the seismic section and get a clear view of various structures and discontinuity in our seismic section.

2.1.2. Generation of time and depth structure maps

Time structure maps were generated using the mapped horizons and fault polygons. From the time structure maps, depth maps were built using the velocity data of the well Fana N_2. The nonlinear function order 3, has a good match and demonstrated no substantial structures on the time and depth surfaces.

3. Results and discussion

3.1. Well correlation and lithology identification

In this study, the first step involves identification of the lithologies on well logs, and then lithostratigraphic well correlation across the Fana Field. Consequently, an unconformity surface is detectable when there is an abrupt increase in gamma-ray, sonic, and resistivity logs. The area where the gamma-ray reading is less than 75 °API was classified as a potential reservoir, while the other part with a high gamma-ray reading (greater than 75 °API) is considered as shale. The lithological interpretation shows the typical stratigraphic sequence of sand and shale across the wells in the field. The five identified reservoir units (E_1, E_2, E_3, E_4, and E_5) were correlated across the four wells namely Fana W_1, Fana N_2, Fana_2, and Fana E_1 (Figure 4).

The average reservoir thickness for E_1, E_2, E_3, E_4, and E_5 include 25.61 m, 46.58 m, 70.42 m, 20.53 m, and 31.98 m respectively. E_4 is the thinness reservoir, while E_2 is the thickest reservoir. The five delineated hydrocarbon reservoir units (E_1, E_2, E_3, E_4, and E_5) are within the Paleogene Sokor_1 Formation as discussed by Genik (1993). In the four drilled exploratory wells in the field, the targeted hydrocarbon reservoirs of E_1 Formation were successfully penetrated at depths of for the wells Fana W_1, Fana N_2, Fana E_1, Fana_2, Fana E_1, respectively at 1306.73-1347.52 m, 1424.65-1435.96 m, 1133.08-1166.76 m, 1159.79-1176.48 m.

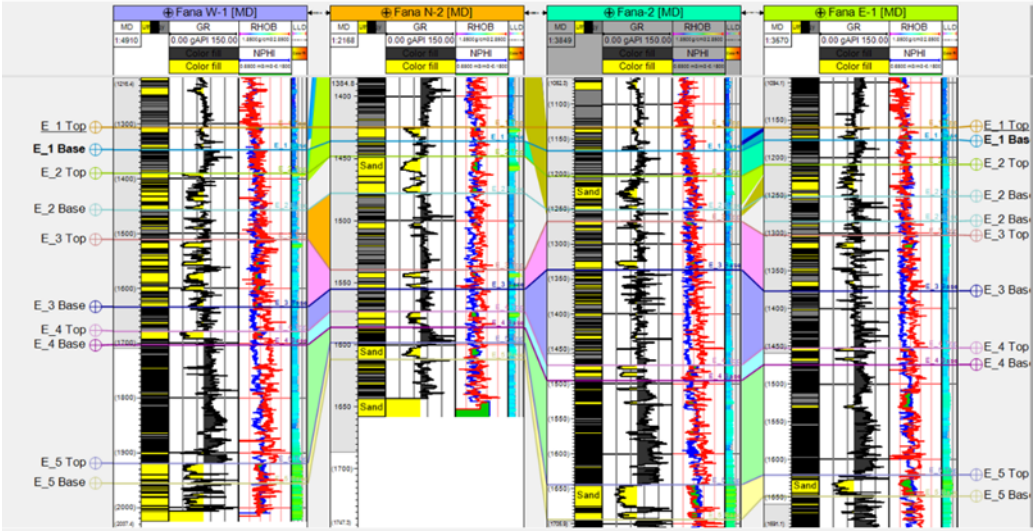

Figure 4. Gamma-ray log and Density-Neutron well correlation of the wells in the study area.
NOTE: Yellow colour for sandstone, black for shale, and grey for shaly sand formations.

3.2. Reservoir petrophysical properties

The reservoir parameters were interpreted for the four wells in the field. Five different reservoirs (E_1, E_2, E_3, E_4, and E_1) were identified. The average resistivity (ILD), bulk density (RHOB), and neutron-porosity hydrogen index (NPHI) were used to identify the oil-bearing units in the reservoir. In this study, well logs were interpreted to estimate the petrophysical characteristics of the reservoir as indicated in Table 2. The gamma-ray, resistivity, sonic, and neutron density logs were integrated to estimate the gross thickness and net pay, volume of shale, hydrocarbon and water saturation, and total and effective porosity.

E_1 Reservoir

The reservoir's thickness varied between 11.31 m and 40.79 m throughout the four wells, with an average gross thickness of 26.61 m, as seen in Table 3. The shale reservoir has an average volume of 5.78%, indicating that it predominantly comprises clean sandstone across the wells. The reservoir exhibited an average net pay of 19.82m and an average net total gas (NTG) content of 73.45%, indicating the existence of hydrocarbon resources in the reservoir. Nevertheless, the net-to-gross (NTG) declined in well Fana N-2, although Fana W-1 exhibits the highest NTG. The reservoir exhibited an average effective porosity of 20.66% and a permeability of 1,774.86 mD. Despite having the lowest average gross thickness, this reservoir has superior quality as determined by several key parameters including V_{sh}, net pay, NTG, porosity, and permeability. Based on the quality of each well, this reservoir has the potential for hydrocarbon production.

E_2 Reservoir

The thickness of the reservoir ranged from 29.8 to 66.72 m throughout the four wells, with an average gross thickness of 46.58 m as seen in Table 3. With an average shale volume of 8.7%, the shale content showed that the purity of this reservoir is comparable to that of sand E_1. Among the four wells, the most favourable reservoir was identified in well Fana W-1, exhibiting an average net pay of 37.88 m and an average net total gas (NTG) content of 79.68 %. The reservoir located in well Fana W-1 shows a net-to-gas (NTG) ratio of 86% indicating a good probable hydrocarbon content. The reservoir indicated an average porosity of 18.79 % and a permeability of 1,535.82 mD. This reservoir exhibits a commendable quality based on [25] and the measurements of V_{sh}, net pay, NTG, porosity, and permeability.

Table 2. Summary of petrophysical parameters computed for the wells.

Well No	Reservoir Sands	Top (m)	Base (m)	Gross Thickness (m)	Vsh (m)	Net Pay (m)	NTG (%)	ØT (%)	ØE (%)	Sw (%)	K (mD)
Fana W-1	E-1	1306.73	1347.52	40.79	7.90	32.89	81	29.69	19.36	35.09	1866.48
	E-2	1390.49	1457.21	66.72	9.57	57.15	86	25.66	14.35	38.94	1684.80
	E-3	1511.24	1634.04	122.8	22.33	100.47	82	23.19	19.23	48.66	1395.10
	E-4	1678.36	1703.37	25.01	4.40	20.61	82	22.27	19.41	59.20	1545.45
	E-5	1919.52	1955.95	36.43	6.01	30.42	83	22.87	2.01	62.12	1519.04
Fana N-2	E-1	1424.65	1435.96	11.31	5.39	5.92	52	25.40	12.75	13.33	1163.94
	E-2	1448.13	1477.93	29.8	9.40	20.40	68	23.74	16.57	57.04	1113.86
	E-3	1539.51	1555.16	15.65	5.84	9.81	63	25.30	16.37	59.04	1141.98
	E-4	1573.1	1585.93	12.83	4.15	8.68	68	25.34	17.45	61.37	1208.12
	E-5	1598.37	1611.77	13.4	4.63	8.77	65	26.40	17.73	55.21	1238.80
Fana-2	E-1	1133.08	1166.76	33.68	6.61	27.07	80	29.87	24.03	34.75	1868.26
	E-2	1202.92	1250.82	47.9	8.13	39.77	83	23.60	19.72	44.70	1406.45
	E-3	1267.65	1336.89	69.24	14.91	54.33	78	23.76	18.76	47.59	1317.38
	E-4	1473.16	1495.24	22.08	5.76	16.32	74	21.50	16.59	66.02	1224.42
	E-5	1644.24	1693.91	49.67	12.73	36.94	74	20.14	16.63	80.55	1285.58
Fana E-1	E-1	1159.79	1176.48	16.69	3.26	13.43	80	32.97	26.51	31.36	2200.77
	E-2	1209.14	1251.07	41.93	7.71	34.22	82	29.99	24.53	34.10	1938.18
	E-3	1302.8	1376.79	73.99	17.51	56.48	76	24.66	18.95	46.08	1345.92
	E-4	1452.34	1474.56	22.22	6.79	15.43	69	23.98	17.13	58.76	1323.69
	E-5	1620.7	1649.15	28.45	9.42	19.03	67	21.87	16.22	80.03	1315.23

Table 3. Average results of the petrophysical parameters of the wells.

Field	Reservoirs	Gross (m)	Net	$^{N}/_{G}$	$Ø_E$ (%)	V_{sh} (%)	S_w (%)	Perm (mD)	Sh (%)
Fana Field	E_1	25.61	19.82	73.45	20.66	5.78	28.63	1774.86	71.37
	E_2	46.58	37.88	79.68	18.79	8.7	43.7	1535.82	56.31
	E_3	70.42	55.27	74.83	18.33	15.14	50.34	1300.09	49.66
	E_4	20.53	15.26	73.36	17.65	5.27	61.34	1325.42	38.66
	E_5	31.98	23.78	72.54	13.15	8.19	69.48	1339.66	30.52

E-3 Reservoir

Table 2 displays the reservoir's thickness, which ranged from 15.65 to 122.8 m throughout the four wells. The average gross thickness is 70.42 m. E_3, with an average shale volume of 15.14%, has the highest shale composition among all the wells. The reservoir has an average net pay of 55.27 m and an average net total gas (NTG) of 74.83%. The reservoir exhibited an average permeability of 1300.09mD and a porosity of 18.33%. Despite possessing the highest average gross thickness.

E-4 Reservoir

The reservoir has a range of thicknesses, spanning from 12.83 to 25.01 m, throughout the four wells. The average gross thickness, as seen in Table 2, is 20.53 m. The cleanliness of this reservoir is marginally superior to that of sand, as evidenced by the average shale volume of 5.27%. The reservoir exhibited an average net pay of 15.26 m and an average NTG of 73.36 %. Throughout the four wells, E_4 demonstrated the lowest net pay thickness. The reservoir exhibited an average porosity of 17.65% and a permeability of 1,325.42 mD. Nevertheless, the reservoir E_4 in the Fana Field meets the criteria for hydrocarbon production, especially in well Fana W-1.

E-5 Reservoir

The reservoir has a range of thicknesses, varying from 13.4 to 49.67 m across the four wells. Table 2 provides an average gross thickness of 31.98 m. The reservoir's shale concentration, with an average volume of 8.19%, indicates that its cleanness is similar to that of E_2. Among the four wells, the reservoir E-5 has the lowest porosity content, which is fair according to [26]. The estimated porosity of the reservoir is 13.15%, while its permeability is measured at 1,339.66 mD. According to [25], this reservoir demonstrates poor characteristics. Across the wells in the field, reservoir E_1 stands out as the best reservoir based on its high hydrocarbon saturation and effective porosity.

3.3. Seismic interpretation

The seismic interpretation involved the mapping of horizons and faults. Fana N_2 seismic well tie results indicated that all reservoir tops are in the sand unit zone. The red horizons are indicated in the shale unit zone. In the synthetic seismogram (Figure 5), the blue horizon (negative amplitude) and red horizon (positive amplitude) represent the trough and the peak respectively. The fault interpretation was carried out at each 10 inline, while the horizons interpretation was mapped at each 25th inline and crossline. The seed grid of faults and horizons was used to generate time surface maps and depth structural maps. Thirty-three (33) major faults were mapped across the field. The identified fault types are normal faults with a complex fault system (Figure 6). The fault system trend is NNW-SSE.

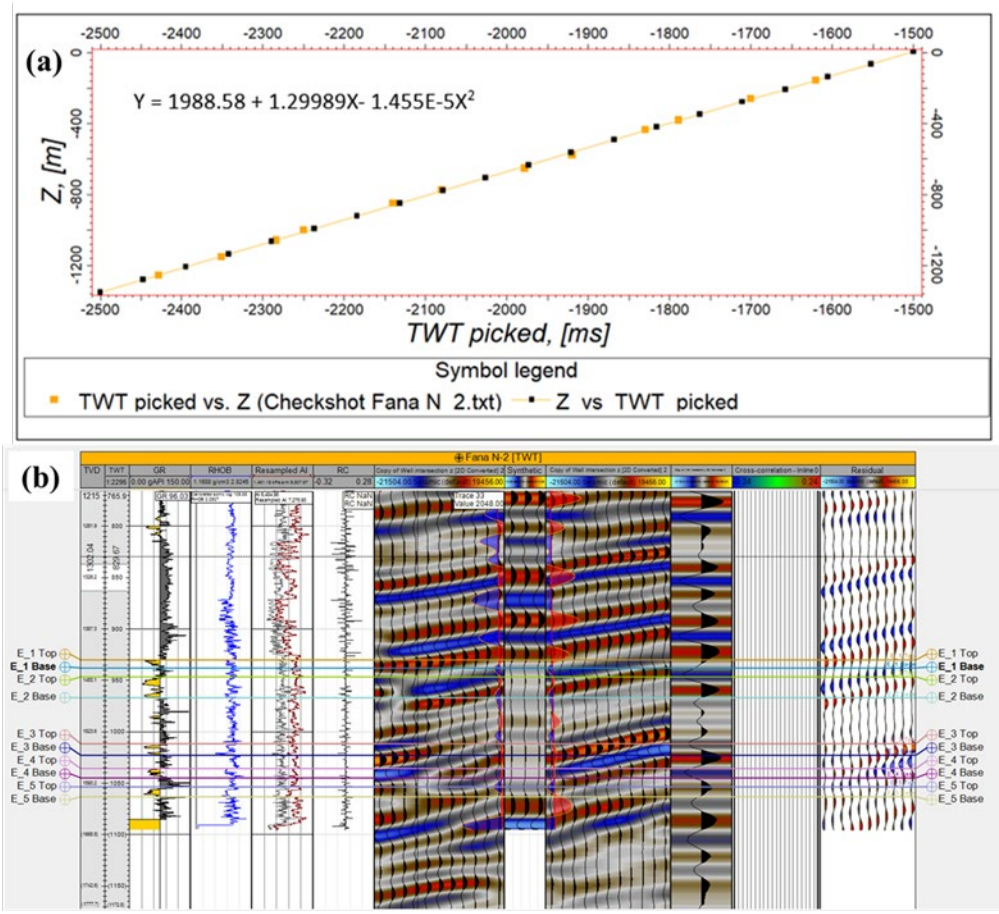

Figure 5. (a) Check-shot profile of the well Fana N_2, and (b) the results synthetic seismogram from the seismic well tie.

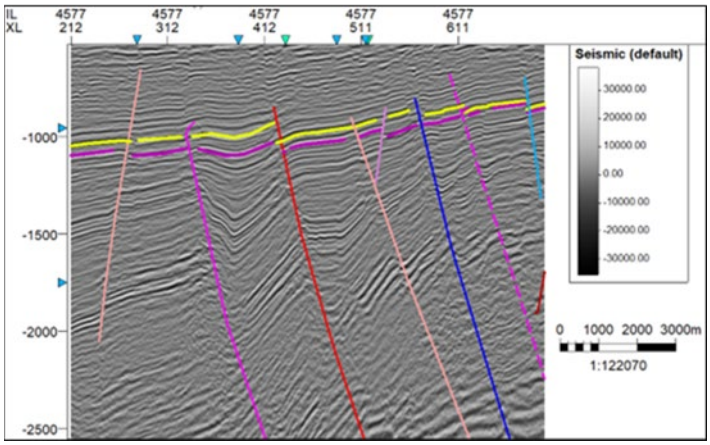

Figure 6. Inline 4577 shows the mapped faults and horizon (top and base) in the study area.

3.4. Time and depth structural maps

The faulted time map was generated from the mapped horizon and fault polygons. The time surface maps showed a travel time ranging from 600 to 1240 ms at a contour interval of 135 ms (Figure 7a). The depth structure maps were then generated for all reservoirs (Figure 7b). However, the difference between time surfaces and the depth surface maps gave reasons for applying the velocity model to carry out the conversion.

The contour interval time and depth structural maps is 300 m. From the mapped horizons and faults, time structural maps have highs and lows (Fig. 8). In the western and central parts of the study area, the reservoir surfaces are faulted most severely. The highs are displayed in orange-yellow colouration while the lows are shown in blue colouration. Since hydrocarbon migrates from lower to higher elevations (purple-blue colouration), the wells in this field are located on high-elevation terrain with closed contours.

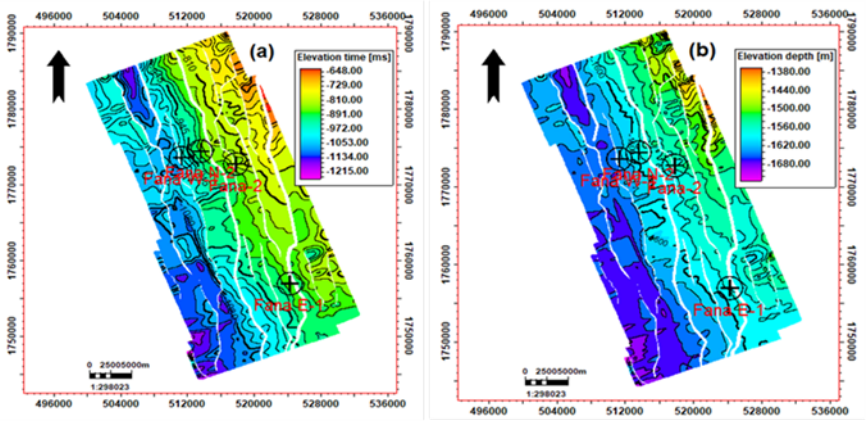

Figure 7. Reservoir top showing Time-Surface map (a), and Depth-Surface map (b).

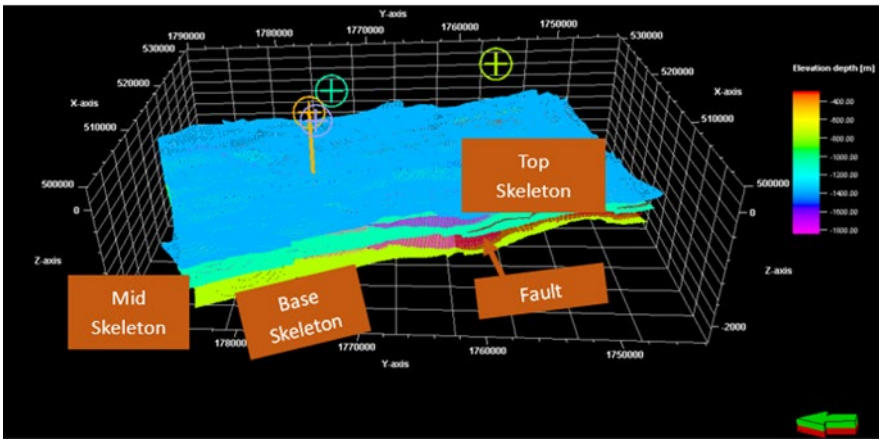

Figure 8. Reservoir Top showing 3D cellular gridding components of the structural model.

3.5. 3D Static models

The 3D structural grids were generated to build the static model of the reservoir (Figure 8). The created structural model shows different orientations of normal faults in the skeleton. This model provides further information gathered from the depth structure map.

The 3D static models were generated for the volume of shale (V_{sh}), porosity (total and effective), water saturation (S_w), and permeability distribution in the Fana Field. The shale volume model indicates that the shale content is higher (24-44%) in the northeast and northwest of the field, and low in the southern part (Figure 9). For the analysis and comparison, the upscaled histogram of water saturation and total porosity is displayed and indicates a very close level as indicated in (Figure 10).

The 3D view of the porosity distribution (effective and total) shows values ranging between 8-21% for the effective porosity and between 17-25% for total porosity in the northern part of the field around well Fana E_1 and Fana_2 (Figure 11; Figure 12). Based on [25], the qualitative description of porosity in this field showed good to very good reservoirs. Therefore, the range of porosity values indicated that sandstone can be considered a good hydrocarbon reservoir. The generated permeability model showed the value was spatially distributed above

1,000 mD which showed excellent reservoir quality across the reservoir (Figure 13). The 3D model showed that all four wells penetrated the hydrocarbon-bearing zones. Meanwhile, the southern parts of the area farther from the well locations demonstrated poor to fair permeability, ranging from 1 to 1000 mD.

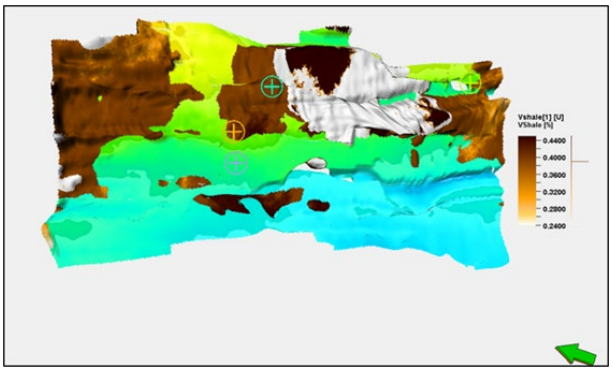

Figure 9. 3D distribution model of the shale volume across Fana Field.

The water saturation model shows the distribution of water in the field. The model showed low water saturation values (10-20%) around well Fana E_1, Fana W_1, and Fan N_2, in the northeast while it is high (40-70%) around well Fana_2 in the north-central part of the Field (Figure 14). The low water saturation areas are expected to have high hydrocarbon saturation. These low water saturation areas are indicative of being saturated with more hydrocarbons while the zones with high water saturation contain less hydrocarbon saturation.

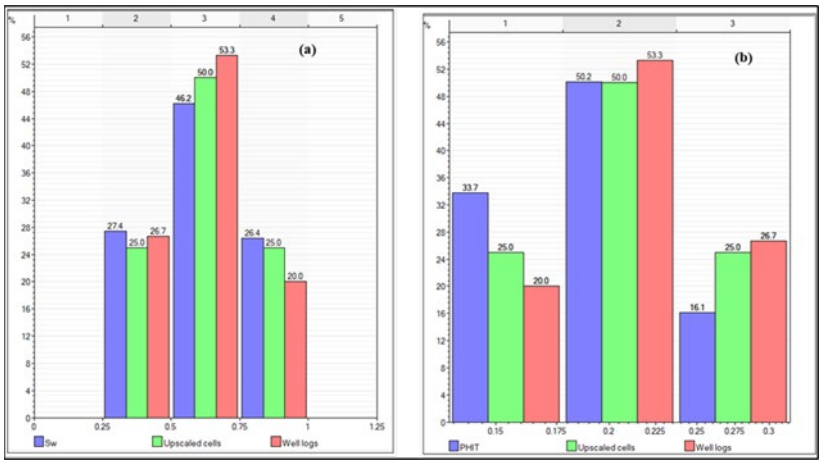

Figure 10. Histogram of upscaled water saturation (S_w) logs model in percentage (a), upscaled and model percentage are in agreement, and upscaled effective porosity (PHIE) logs model in decimal.

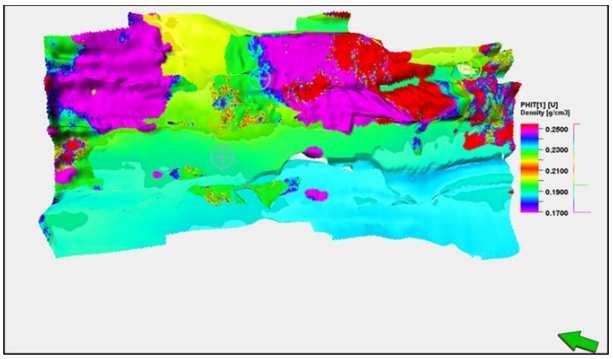

Figure 11. The 3D distribution model of the total porosity across Fana Field.

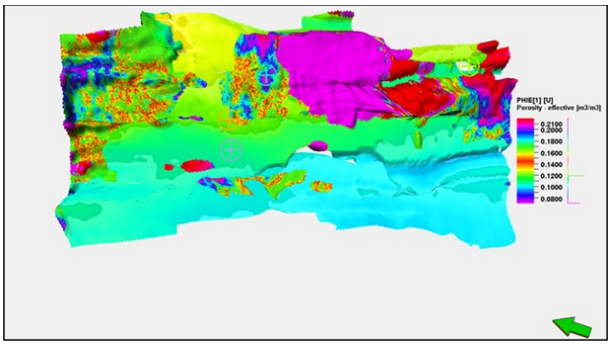

Figure 12. The 3D distribution model of the effective porosity across Fana Field.

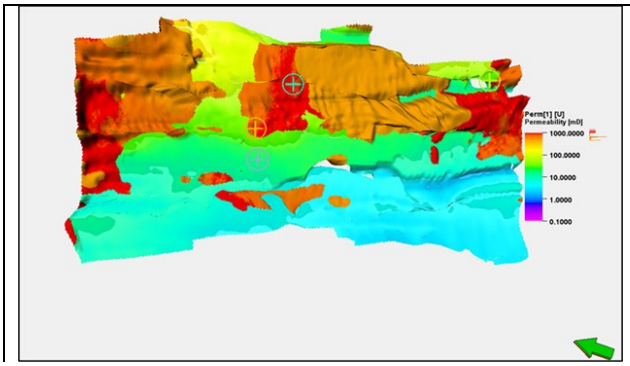

Figure 13. The 3D distribution model of the permeability across Fana Field.

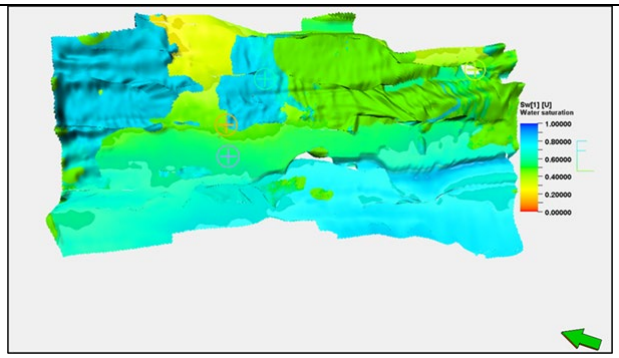

Figure 14. The 3D distribution model of water saturation.

3.6. Implications on hydrocarbon prospectivity

The sandstone of the Paleogene Sokor-1 Formation has mainly quartz (> 90%), feldspar, and rock debris and can be regarded as highly compositional mature sandstone [27]. The sandstones interbedded with shale members of the Sokor-1 Formation in the Termit Basin have good porosity values (average porosity of 20% - 28%), and permeability from 250 md to 1 Darcy [11]. The reservoirs of the Sokor-1 Formation are less than 1,200 m deep in the Trakes slope, with porosity ranging from 25% - to 30%, nearly all of the reservoirs of the Sokor-1 Formation in Termit Basin possess medium to high porosity [27].

The computed results obtained through petrophysical evaluation indicated that all the delineated hydrocarbon-bearing reservoirs in the Fana Field have good porosity and permeability values and are hydrocarbon-saturated with potential for hydrocarbon production. The mapped NW-SW and NNW-SSE trending faults could have served as migration paths for Cretaceous (Donga and Yogou Formation)-sourced oil into Paleogene Sokor-1 sandstones or younger reservoir units. This study showed the relevance of well logs and seismic data for delineating structures and 3D models for hydrocarbon accumulation [28-29].

4. Conclusion

This study utilized well logs and seismic data to provide subsurface information on the petrophysical properties of identified sand bodies across the Termit Basin of the Niger Republic. The petrophysical properties namely net-to-gross, volume of shale, porosity, permeability, and fluids saturation were evaluated. Five (5) identified reservoirs (E_1, E_2, E_3, E_4, and E_5) were significantly defined, where E_1 stands as the best reservoir with low water saturation, good porosity, and permeability. helped to confirm the presence of good reservoir-quality sand in the identified reservoirs.

The seismic interpretation was done to complete reservoir evaluation by generating a 3-D static model of the reservoir in the Fana Field. The structural system and discontinuity of the studied field were identified using seismic interpretation. The structural interpretation revealed that the Termit basin is highly faulted and reservoirs are mainly faulted-assisted traps. The interpreted faults are mostly normal and oriented in directions NW-SW and NNW-SSE.

This study has shown that the reservoir properties distribution in the Fana Field from the generated model gives confidence of a good hydrocarbon accumulation.

Acknowledgements

The authors extend their gratitude to the Centre of Petroleum Documentation, Niger Republic for providing the data used in this study. The authors acknowledge the African Union Commission for providing funding to conduct this research study. We appreciate GCube Integrated Services Ltd, Lagos, Nigeria for providing a subsurface workstation and license used during the modelling.

Funding: *This research was supported by the African Union Commission through the Pan African University Life and Earth Sciences Institute (Including Health and Agriculture), Ibadan, Nigeria.*

***Conflict of interest**: The authors have declared that no competing interests exist.*

References

[1] Browne SE, and Fairhead JD. Gravity Study of the Central African Rift System: A Model of Continental Disruption. Part 1: The Ngaoundéré and Abu Gabra Rifts. In: Morgan, P. and Baker, B.H., Eds., Developments in Geotectonics, Elsevier, Amsterdam, 1983; 19(3): 187-203. https://doi.org/10.1016/B978-0-444-42198-2.50018-3 .

[2] Genik GJ. Regional framework, structural and petroleum aspects of rift basins in Niger, Chad and the Central African Republic (C. A. R.). In geodynamics of rifting, Elsevier, 1992; 2(213): 169-185. https://doi.org/10.1016/B978-0-444-89912-5.50036-3

[3] Genik GJ. Petroleum Geology of Cretaceous-Tertiary Rift Basins in Niger, Chad and Central African Republic. In Bulletin of American Association of Petroleum Geologists, 1993; 75(8): 1405–1434.

[4] Liu B, Bo J, Mo L, Mao F, Liu J, LV M, Wang Y, Chen Z, Jiang. Polyphase Rift Evolution of the Termit Basin, Eastern Niger: Constraints from Structural and Sedimentary Records. Geoscience, 2012; 26(2): 317–325.

[5] Lai H, Li M, Liu J, Mao F, Xiao H, He W, Yang L. Organic geochemical characteristics and depositional models of Upper Cretaceous marine source rocks in the Termit Basin, Niger. Journal of Palaeogeography, 2018; 495(18): 292–308. https://doi.org/10.1016/j.palaeo.2018.01.024

[6] Lai H, Li M, Mao F, Liu J, Xiao H, Tang Y, Shi S. Source rock types, distribution and their hydrocarbon generative potential within the Paleogene Sokor-1 and LV formations in Termit Basin, Niger. Energy Exploration and Exploitation, 2020; 38(6): 2143–2168. https://doi.org/10.1177/0144598720915534

[7] Zhou L, Su J, Dong X, Shi B, Sun Z, Qian M, Lou D, Liu A. Controlling factors of hydrocarbon accumulation in Termit rift superimposed basin, Niger. Petroleum Exploration and Development, 2017; 44(3): 358–367. https://doi.org/10.1016/S1876-3804(17)30042-3

[8] Nasaruddin MN, Zung L.S. and Rafek, AGM. Petrophysical Analysis of E5 Sand Group of Sokor Formation, Termit Basin, Niger. IOP Conference Series: Earth and Environmental Science, 2017; 88(1): 012003, https://doi.org/10.1088/1755-1315/88/1/012003

[9] Chang E. and Zung LS. 3D Reservoir Characterization of Field Deta, Termit Basin, Niger. In: Awang., Proceedings of the International Conference on Integrated Petroleum Engineering and Geosciences, Springer, Berlin, 2017, 323–335. https://doi.org/10.1007/978-981-10-3650-728

[10] Zhao X, Jin F, Li Y, Wang Q, Zhou L, Ly Y, Pu X, Wang W. Slope belt types and hydrocarbon migration and accumulation mechanisms in rift basins. Petroleum Exploration and Development, 2016; 43(6): 841–849.

[11] Ahmed K, Liu K, Paterne M, Kra K, Kuttin A, Malquaire K. and Ngum K. Anatomy of Eastern Niger Rift Basin with Specific References of Its Petroleum Systems. International. Journal of Geoscience, 2020; 11(05): 305–324.

[12] Mao F, Jiang H, Ou Y, Cheng X, Yuan S, Wang Y, Zheng F, Li Z. 3D structural modelling and its application in the Termit Basin, Niger. Journal of Earth Science. Front, 2018; 25(2): 62-71.

[13] Abdelwahhab and A. Raef. Integrated reservoir and basin modelling in understanding the petroleum system and evaluating prospects: The Cenomanian reservoir, Bahariya Formation, at Falak Field, Shushan Basin, Western Desert, Egypt. Journal of Petroleum Science and Engineering, 2020; 189:1-27. https://doi.org/10.1016/j.petrol.2020.107023

[14] El-Gawad E, Abdelwahhab M, Bekiet M, Nooh A, Elsayed N, Fouda A. Static reservoir modeling of El Wastani formation, for justifying development plans, using 2D seismic and well log data in Scarab field, offshore Nile Delta Egypt. Journal of African Earth Science, 2019; 158. DOI: 10.1016/j.jafrearsci.2019.103546.

[15] Wang W, Wang T, Li M, Mao F, Liu J, Xiao, H, Lai H, Ai X. The origins of biodegraded oils in sandstone reservoirs in the Termit Basin. Journal of Petroleum Science and Engineering, 2021; 109-130. https://doi.org/10.1016/j.petrol.2021.109130

[16] Xiao H, Wang T. G, Li M, Lai H, Liu J, Mao F, Tang Y. Geochemical characteristics of Cretaceous Yogou Formation source rocks and oil-source correlation within a sequence stratigraphic framework in the Termit Basin, Niger. Journal of Petroleum Science and Engineering, 2019; 360–372. https://doi.org/10.1016/j.petrol.2018.09.082

[17] Zanguina M, Bruneton A, Gonnar R. An introduction to the petroleum potential of Niger. Journal of Petroleum Geology, 1998; 21(1): 83–103. https://doi.org/10.1111/j.1747-5457.1998.tb00647.x
[18] Harouna M, Pigott J. D, Philp R. P. Burial History and Thermal Maturity Evolution of the Termit Basin, Niger. Journal of Petroleum Geology, 2017; 40(3): 277–297. https://doi.org/10.1111/jpg.12676
[19] Wang X, Wan L, Jiang Z, Liu R, Wang X, Tang W, Gao Y, Liu S, Xu W. Controlling factors and accumulation model of hydrocarbon reservoirs in the Upper Cretaceous Yogou Formation, Koulele Area, Termit Basin, Niger. Journal of Earth Science, 2017; 28(6): 1126–1134. https://doi.org/10.1007/s12583-016-0936-5
[20] Liu J, Li M, Mao F. Reservoir geochemistry in Termit Basin, Central and West Africa rift system. Beijing: Petroleum Industry Press, 2020; 5.
[21] Liu B, Bo JH, Mo LK, Mao F.J, Liu J, LV M.Q, Wang Y. Marine transgression of the eastern Niger Basin in the late Cretaceous: Paleontological and geochemical evidence. Geoscience, 2011; 25(5): 995–1006.
[22] Liu, Zhang G, Mao F, Liu J, Lü M. Geochemistry and Origin of Upper Cretaceous Oils from the Termit Basin, Niger. Journal of Petroleum Geology, 2017; 40(2): 195–207. https://doi.org/10.1111/jpg.12672
[23] Liu R. The sedimentary system of Upper Cretaceous in Termit Basin, Niger. Beijing: China University of Geosciences (Beijing). 2017
[24] Liu B, Pan X, Wan L, Su Y, Mao F, Liu J, Lü M, Wang Y. Structural evolution and main controlling factors of the Paleogene hydrocarbon accumulation in Termit Basin, eastern Niger Acta Petrolei Sinica, 2012; 33(3):394-403.
[25] Rider MH. The Geological Interpretation of Well Logs. In Rider-French Consulting Ltd, 1986; 1: 6605939.
[26] Schlumberger. Log Interpretation Charts, Chart K 3. Schlumberger wireline and Testing, Houston, Texas, 1997; 4–39.
[27] Yuan S, Dou L, Cheng D, Mao F, Pan C, Zheng F, Jiang H, Pang W, Li Z. New understanding and exploration direction of hydrocarbon accumulation in Termit Basin, Niger. Petroleum Exploration and Development, 2023; 50(2): 268–280. https://doi.org/10.1016/S1876-3804(23)60386-6
[28] Igonoh DA, Nwankwo CN. Mapping of Structural traps as a tool for hydrocarbon prospectivity of the K-Field of the Niger Delta, Nigeria. Journal of Petroleum and Coal, 2023; 65(4): 1251-1260.
[29] Oluwajana OA. Petrophysical analysis of Reservoirs in Well-Y, Coastal Swamp Depobelt, Niger Delta Basin, Nigeria. Achievers Journal of Scientific Research, 2022. 4(1):11-20.

To whom correspondence should be addressed: Abass Yacoubou Issaka, Petroleum Geoscience Program, Pan African University Life and Earth Sciences Institute (including Health and Agriculture), University of Ibadan, Ibadan, Nigeria, E-mail: bassyacoubou573@gmail.com